BRIEF DEFINITIVE REPORT

The ubiquitin-editing enzyme A20 controls NK cell homeostasis through regulation of mTOR activity and TNF

Jessica Vetters[1,2,3,4]*, Mary J. van Helden[1,4]*, Sigrid Wahlen[5], Simon J. Tavernier[1,4] (iD), Arne Martens[6,9], Farzaneh Fayazpour[2,3,4], Karl Vergote[1,4], Manon Vanheerswynghels[1,4], Kim Deswarte[1,4], Justine Van Moorleghem[1,4], Sofie De Prijck[1,4], Nozomi Takahashi[6,7], Peter Vandenabeele[6,7] (iD), Louis Boon[8] (iD), Geert van Loo[6,9] (iD), Eric Vivier[10,11] (iD), Bart N. Lambrecht[1,3,4,12]** (iD), and Sophie Janssens[2,3,4]** (iD)

The ubiquitin-editing enzyme A20 is a well-known regulator of immune cell function and homeostasis. In addition, A20 protects cells from death in an ill-defined manner. While most studies focus on its role in the TNF-receptor complex, we here identify a novel component in the A20-mediated decision between life and death. Loss of A20 in NK cells led to spontaneous NK cell death and severe NK cell lymphopenia. The few remaining NK cells showed an immature, hyperactivated phenotype, hallmarked by the basal release of cytokines and cytotoxic molecules. NK-A20$^{-/-}$ cells were hypersensitive to TNF-induced cell death and could be rescued, at least partially, by a combined deficiency with TNF. Unexpectedly, rapamycin, a well-established inhibitor of mTOR, also strongly protected NK-A20$^{-/-}$ cells from death, and further studies revealed that A20 restricts mTOR activation in NK cells. This study therefore maps A20 as a crucial regulator of mTOR signaling and underscores the need for a tightly balanced mTOR pathway in NK cell homeostasis.

Introduction

Natural killer (NK) cells are the cytotoxic members of the heterogeneous population of innate lymphoid cells (ILCs; Vivier et al., 2018). NK cells kill target cells via the binding of death receptors or by the release of lytic granules that contain granzymes and perforin. They also regulate the function of other immune cells by producing chemokines and cytokines such as TNF and IFNγ (Vivier et al., 2008). Under normal conditions, their activation is inhibited by ligands expressed on healthy cells that engage germline-encoded inhibitory receptors on the NK cells. Viral infection (Waggoner et al., 2016), malignant transformation (Vivier et al., 2012), or cellular stress (Raulet and Guerra, 2009) can lead to up-regulation of ligands that are recognized by a vast array of activating receptors. The relative balance of inhibitory and activating signals eventually determines the activity of the NK cell. Several signaling pathways have been identified to play a crucial role in NK cell functioning.

Recently, the mechanistic target of rapamycin (mTOR) pathway was shown to be a hallmark of NK activity (Marçais et al., 2014, 2017). Although NK cell activation has been studied thoroughly, relatively little is known about how activated NK cells are switched off after termination of an inflammatory response.

The NF-κB family of transcription factors plays a key role in inflammatory responses triggered by a plethora of signaling receptors. NF-κB dimers induce expression not only of a large proinflammatory gene program, but also of their own negative regulators, such as inhibitor of κB (IκB) or A20 (encoded by the gene TNFα induced protein 3 (Tnfaip3; Renner and Schmitz, 2009). Absence of A20 leads to prolonged NF-κB activation and elevated production of inflammatory cytokines (Catrysse et al., 2014). A20-deficient mice show widespread tissue inflammation and perinatal death (Lee et al., 2000). Also in humans, polymorphisms in the Tnfaip3 gene are

[1]Laboratory of Immunoregulation and Mucosal Immunology, VIB Center for Inflammation Research, Ghent, Belgium;   [2]Laboratory for Endoplasmic Reticulum Stress and Inflammation, VIB Center for Inflammation Research, Ghent, Belgium;   [3]GROUP-ID Consortium, Ghent University and Ghent University Hospital, Ghent, Belgium;   [4]Department of Internal Medicine and Pediatrics, Ghent University, Ghent, Belgium;   [5]Department of Diagnostic Sciences, Ghent University, Ghent, Belgium;   [6]Department of Biomedical Molecular Biology, Ghent University, Ghent, Belgium;   [7]Molecular Signaling and Cell Death, VIB Center for Inflammation Research, Ghent, Belgium;   [8]Bioceros BV, Utrecht, Netherlands;   [9]Cellular and Molecular (Patho)physiology, VIB Center for Inflammation Research, Ghent, Belgium;   [10]Innate Pharma Research Laboratories, Innate Pharma, Marseille, France;   [11]Aix-Marseille University, Assistance Publique–Hôpitaux de Marseille, Centre d'Immunologie de Marseille-Luminy, Hôpital de la Timone, Marseille Immunopôle, Marseille, France;   [12]Department of Pulmonary Medicine, Erasmus University Medical Center, Rotterdam, Netherlands.

*J. Vetters and M.J. van Helden contributed equally to this paper;   **B.N. Lambrecht and S. Janssens contributed equally to this paper;   Correspondence to Sophie Janssens: sophie.janssens@irc.vib-ugent.be;   Bart N. Lambrecht: bart.lambrecht@irc.vib-ugent.be.

associated with a number of inflammatory and autoimmune conditions (Catrysse et al., 2014). Conditional deletion of A20 in a vast array of cell types revealed that loss of A20 is associated with exacerbated inflammatory responses and, depending on the cell type, autoimmunity (for references, see Catrysse et al., 2014). In addition, A20 plays a critical role in the development and differentiation of lymphocytes (Chu et al., 2011; Onizawa et al., 2015; Drennan et al., 2016). Besides its role in regulating inflammation, A20 protects cells from necroptosis and TNF-induced apoptosis, in an as yet ill-defined manner (Opipari et al., 1992; Lee et al., 2000; Vereecke et al., 2010; Onizawa et al., 2015; Catrysse et al., 2016).

Being guarded by a delicate balance between inhibitory and activating signals, NK cells might be particularly sensitive to a regulator such as A20, and we here set out to determine A20's role in NK cells by specific ablation using Cre-lox technology. Unexpectedly, Ncr1 (NKp46)-mediated deletion of A20 led to severe NK cell lymphopenia. The few A20-deficient remaining NK cells were hyperactive and more sensitive to TNF-induced cell death. Furthermore, A20-deficient NK cells showed high baseline activation of the mTOR signaling pathway, and treatment with rapamycin in vivo rescued A20-deficient cells from death. Our data therefore classify A20 as a bona fide regulator of mTOR signaling and show that a tight regulation of mTOR signaling is crucial for proper NK cell homeostasis.

Results and discussion

Absence of A20 leads to severe NK cell lymphopenia

NK-A20$^{-/-}$ mice were generated by crossing $Ncr1^{iCre/+}$ mice (Narni-Mancinelli et al., 2011) to mice bearing loxP-flanked exons IV and V of the A20 gene (Vereecke et al., 2010), leading to loss of A20 in all NKp46$^+$ cells (Fig. 1 A). NK-A20$^{-/-}$ mice were born at normal Mendelian inheritance and developed to adulthood normally. Gene expression analysis confirmed specific loss of A20 in NK cells only (Fig. 1 A). Immunophenotyping of the NK-A20$^{-/-}$ mice revealed an almost complete absence of NK cells in all organs examined (Fig. 1 B). The A20-mediated effect was not dose dependent, as intermediate levels of A20 in the NK-A20$^{+/-}$ mice (Fig. 1 A) were sufficient for proper NK cell homeostasis (Fig. 1, B and C). Neither T or B cells, nor any other immune cell population, were affected in NK-A20$^{-/-}$ mice (Figs. 1 A and S1 B). A few other NKp46$^+$ ILC subsets, ILC1s and ILC3s, also become targeted by the Ncr1-promotor driven Cre expression (Narni-Mancinelli et al., 2011). ILC1s, a relatively abundant population of ILCs in the liver, were also drastically affected by the loss of A20, while proportions of ILC3s in the lamina propria of the small intestine (LP-SI) remained unaltered (Fig. S1, C–F). In both liver and LP-SI, conventional NK cells (cNKs) were affected, confirming widespread NK cell lymphopenia.

The generation of bone marrow (BM) chimeras (Fig. 1 D) confirmed that the observed defect in NK cell survival was cell intrinsic and that, again, no effect could be observed in NK-A20$^{+/-}$ cells (Fig. 1, E–G). In conclusion, these data show that complete absence of A20 in NK cells results in severe NK lymphopenia, in a cell-intrinsic manner.

A20-deficient NK cells are hyperactive

NK cells differentiate through a series of maturation stages, which can be traced in vivo by the sequential acquisition and loss of specific cell surface receptors. Immature NK cells are defined by the presence of CD27 and absence of CD11b (CD11b^{lo}), while fully mature NK cells gain CD11b and lose CD27 expression (CD27^{lo}; Kim et al., 2002; Hayakawa and Smyth, 2006; Chiossone et al., 2009; Fig. 2 A). Although NK cell numbers were severely decreased in each maturation stage (Fig. 2 A, lower panel), the relative proportions of the different substages changed dramatically, and residual NK cells in the spleen of NK-A20$^{-/-}$ mice displayed a marked shift toward the immature phenotype (Fig. 2 A, contour plot and middle panel). Furthermore, A20-deficient NK cells showed a highly proliferative phenotype as assessed by Ki-67 expression (Fig. 2 B, upper panel). This enhanced proliferation was not a direct consequence of having lower numbers of NK cells in an attempt to fill up the empty niche, as A20-deficient NK cells in mixed BM chimeric mice reconstituted with WT and NK-A20$^{-/-}$ BM also showed increased Ki-67 expression (Fig. 2 B, lower panel).

We then performed functional studies and tested intracellular IFNγ production and degranulation, as measured by cell-surface CD107a expression, a lysosomal marker that translocates to the cell surface upon degranulation (Alter et al., 2004). Even without prior stimulation, NK-A20$^{-/-}$ mice displayed a hyperactive phenotype as revealed by the enhanced proportion of CD107a$^+$ and IFNγ$^+$ NK-A20$^{-/-}$ cells in steady state (Fig. 2 C). Ex vivo restimulation with plate-bound antibodies against NK1.1 or with the cytokines IL-12/IL-18 or IL-12/IL-2 triggered a higher degree of degranulation in the absence of A20. The proportion of IFNγ$^+$ cells was not altered, but we noticed that IFNγ expression levels on a per-cell basis were strongly elevated in NK-A20$^{-/-}$ cells (Fig. 2 C). Finally, we also assessed NF-κB activation, using phosphorylation of Ser536 on p65 (P-p65) as readout. Both in steady state and upon TNF activation, levels of P-p65 were markedly increased in the absence of A20 (Fig. 2 D), as expected from A20's known NF-κB inhibitory function.

In summary, these data show that the few remaining NK cells in the NK-A20$^{-/-}$ mice showed a relatively immature phenotype but were hyperactive, as revealed by increased proliferation, increased cytokine production, increased degranulation, and increased signs of NF-κB activation, both in steady state and upon ex vivo restimulation.

A20 is indispensable for NK cell survival

Our results thus far showed that NK-A20$^{-/-}$ mice have severe NK cell lymphopenia. To assess whether A20 might affect NK cell survival, we first examined the viability of freshly isolated splenocytes by staining with annexin V and a viability marker. We consistently measured decreased viability of A20-deficient NK cells, accompanied by slightly activated caspase 3 levels (Fig. S2, A and B). To follow the fate of NK-A20$^{-/-}$ cells over time, we generated a tamoxifen-inducible A20 knockout mouse by crossing LoxP-flanked A20 mice to the ERT2-Cre$^{tg/+}$ mouse line. As full A20 deletion is lethal (Lee et al., 2000), we enriched NK cells from the spleens of these mice (CD45.2 A20$^{fl/fl}$ × ERT2-Cre$^+$ or ERT2-Cre$^-$) and mixed them with enriched NK cells from
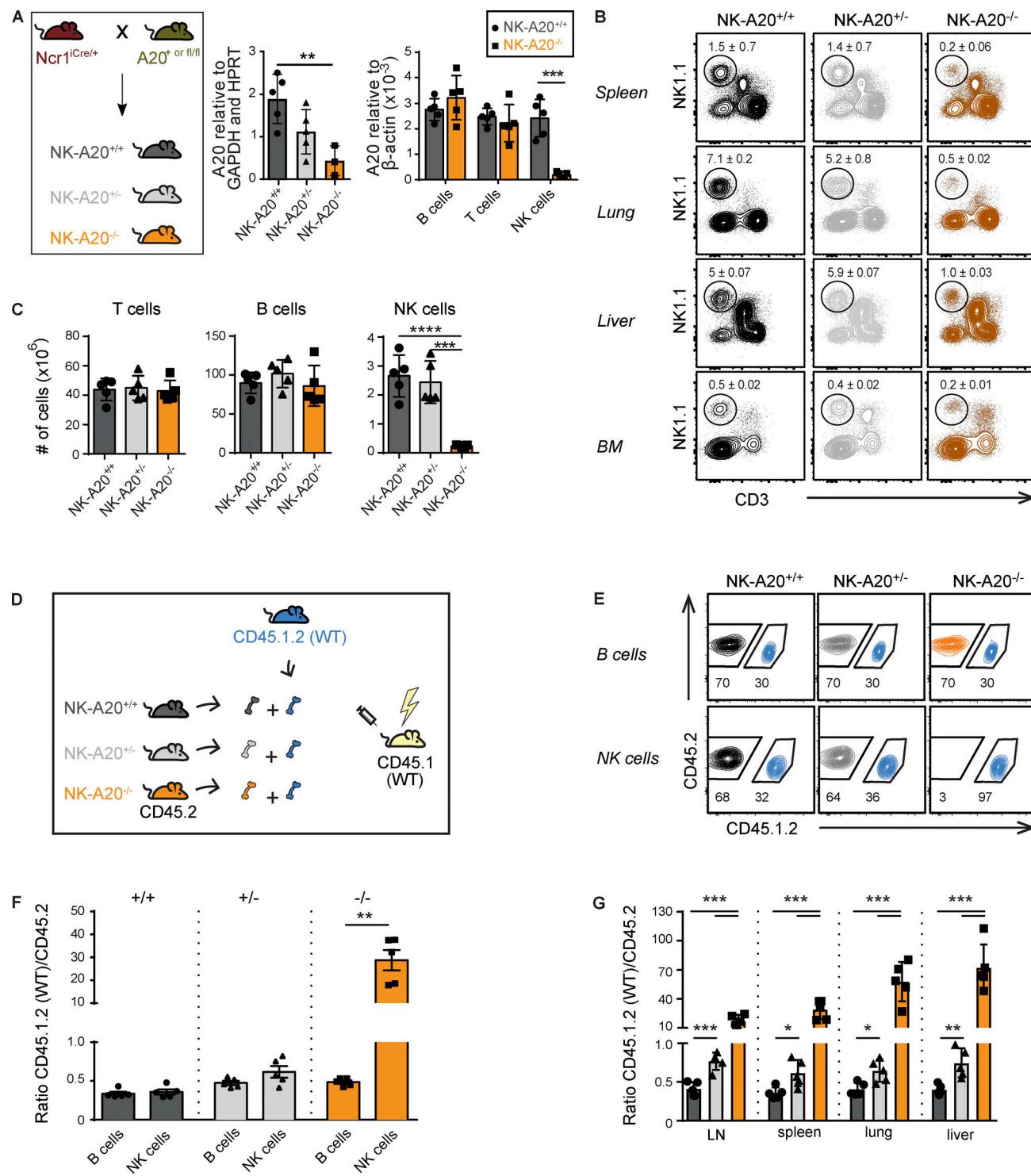
Vetters et al.
A20 controls NK homeostasis through mTOR and TNF

Journal of Experimental Medicine
https://doi.org/10.1084/jem.20182164

2011

Figure 1. **Genetic ablation of A20 in NKp46⁺ cells leads to severe NK cell lymphopenia. (A)** Graphical representation and validation by RT-qPCR of the NK-A20 mouse model. Bar graphs represent A20 RNA expression as measured in sorted splenic lymphocyte populations. Expression was normalized to the indicated housekeeping genes. **(B and C)** Flow cytometry analysis to assess NK cell percentages in the indicated organs and absolute numbers of splenic lymphocyte populations in NK-A20 mice. **(D)** Graphical representation of NK-A20 mixed BM chimeric setup. **(E–G)** FACS plots and bar graphs represent percentages or ratios of CD45.1.2⁺ and CD45.2⁺ B cells or NK cells as retrieved from the spleens or indicated organs of mixed BM chimeras. For all figures, bar graphs represent mean ± SD, and dots represent individual mice. Data are representative of at least two independent experiments, with the exception of A, middle panel. Unpaired Student's t tests: *, $P < 0.05$; **, $P < 0.01$; ***, $P < 0.001$; ****, $P < 0.0001$.
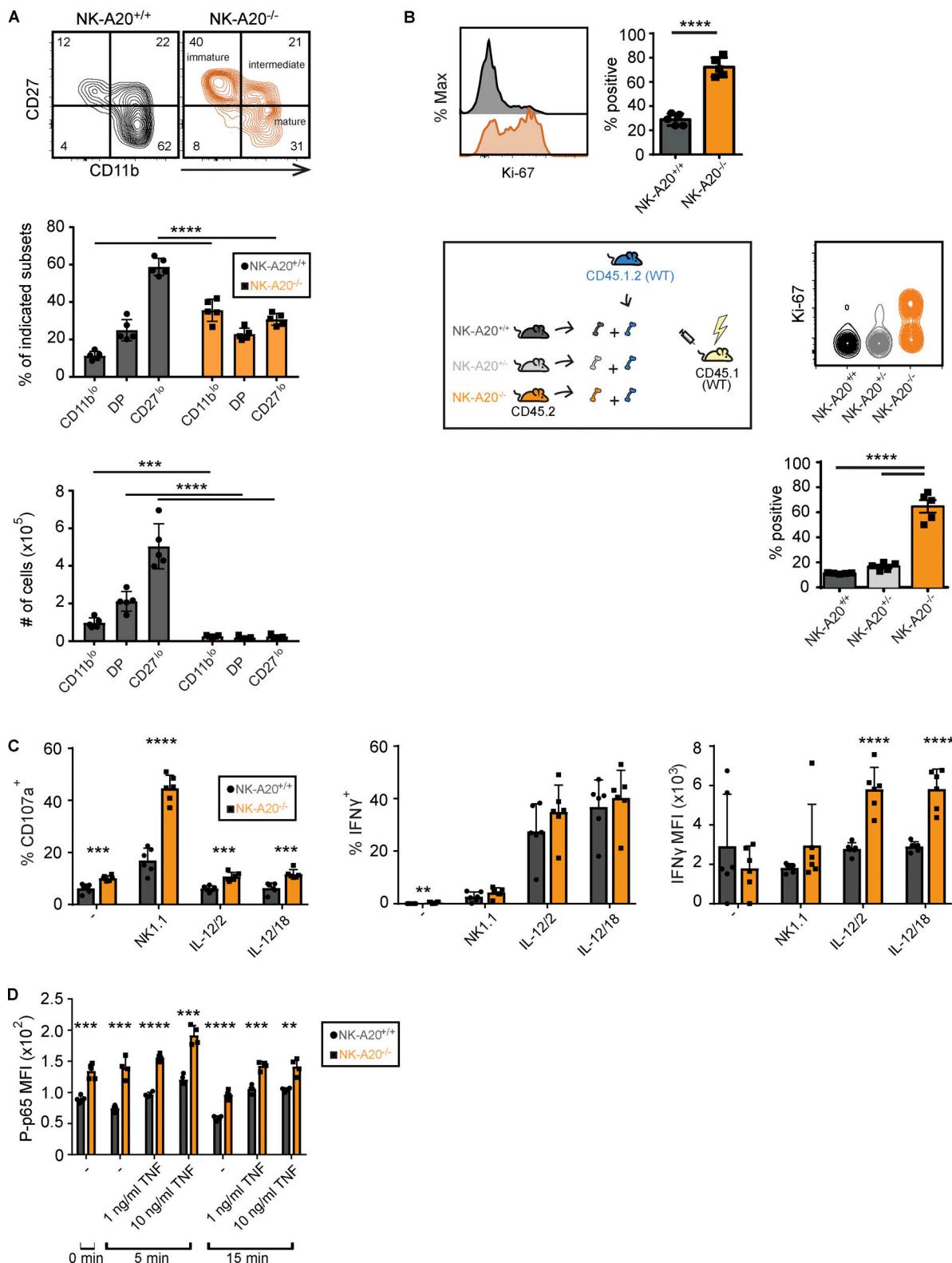
Figure 2. Loss of A20 renders NK cells relatively immature and highly hyperactive. (A–D) Flow cytometry analysis of splenic NK cells isolated from NK-A20 mice. **(A)** FACS plots and bar graphs represent percentages and absolute numbers of NK cell subsets, determined by CD11b/CD27 expression. CD11b^{lo}, CD11b^{lo}CD27^{hi}, immature; DP, CD11b^{hi}CD27^{hi}, double positive (DP) or intermediate; CD27^{lo}, CD11b^{lo}CD27^{hi}, mature. **(B)** Ki-67 expression as measured in splenic NK cells from NK-A20 mice (top) or mixed BM chimeric mice (bottom). **(C)** Bar graphs depict percentages of CD107a$^+$ or IFNγ$^+$ NK cells and IFNγ geometrical mean fluorescence intensity (MFI) within IFNγ$^+$ NK cell population. **(D)** P-p65 MFI on gated splenic NK cells as measured by phosphoflow immediately after isolation or upon TNF stimulation. For all figures, bar graphs represent mean ± SD, and dots represent individual mice. Data are representative of at least two independent experiments. Unpaired Student's t test: **, $P < 0.01$; ***, $P < 0.001$; ****, $P < 0.0001$.

CD45.1 congenic control mice (Fig. 3 A). This mix was adoptively transferred to CD45.1.2 congenic acceptor mice that were subsequently injected i.p. with tamoxifen for 5 d consecutively. Acceptor mice were bled on days 1, 4, 7, and 10 to determine the ratio of CD45.2 to CD45.1 donor NK cells, which was compared to the ratio before injection (Fig. 3 A, flow panels and survival curve). This analysis showed that upon tamoxifen injection, ERT2-Cre$^+$ NK cells lost A20 expression from day 2 onwards (Fig. 3 A, bar graph) and were rapidly depleted, unequivocally demonstrating the essential role for A20 in NK cell survival (Fig. 3 A).

NK cell homeostasis depends on IL-15 signaling, which drives expression of the antiapoptotic protein Mcl-1 and inhibits expression of proapoptotic Bim (Huntington et al., 2007; Sathe et al., 2014). Under IL-15–depriving conditions, this delicate balance of pro- and antiapoptotic Bcl-2 family members is disturbed: Bim and Noxa levels rise, while Mcl-1 levels go down. Ectopic Bcl-2 expression restores this balance and can inhibit NK cell apoptosis (Cooper et al., 2002; Minagawa et al., 2002). To determine potential changes in expression of Bcl-2 family members in the absence of A20, we analyzed their expression specifically in the CD11b^{lo} subset, to avoid any potential bias due to the skewed maturation of A20$^{-/-}$ NK cells. While levels of Bcl-2, Bcl-xL, Mcl-1, XIAP, cIAP1, and Bim appeared largely unaffected, we found a marked increase in the levels of the proapoptotic molecule Noxa in A20$^{-/-}$ NK cells (Fig. S2 C). To determine if Bcl-2 can restore NK cell survival in the absence of A20, NK-A20$^{-/-}$ mice were crossed with *H2K-bcl-2* transgenic mice expressing human Bcl-2 in all hematopoietic cells including NK cells (Domen et al., 1998). Bcl-2$^{Tg/+}$ mice displayed splenomegaly, and numbers of splenic NK cells were elevated compared with littermate control mice, as described for other hematopoietic cells (Domen et al., 2000). Notably, the NK cell fold expansion induced by ectopic Bcl-2 expression was significantly higher in A20$^{-/-}$ compared with A20$^{+/+}$ NK cells (7.6- vs. 1.5-fold; Fig. 3 B, lower panel), suggesting that A20-deficient NK cells die, at least partially, through an apoptotic pathway dependent on proapoptotic BH3-only proteins. NK cell numbers were never completely rescued by overexpression of Bcl-2, suggesting that other Bcl-2 family members such as Mcl-1 might play a nonredundant role or that other pathways independent of the intrinsic apoptotic pathway are relevant as well for cell death induced by loss of A20.

Recently, it was shown that in activated T lymphocytes, A20 ubiquitinates receptor-interacting serine/threonine protein kinase 3 (RIPK3) and, as such, protects T cells from dying by necroptosis (Onizawa et al., 2015). To assess whether A20-deficient NK cells also die by necroptosis, we first used a chemical approach relying on the use of the RIPK1 inhibitor necrostatin, a well-established inhibitor of necroptosis (Degterev et al., 2008). As can be seen in Fig. S2 D, treatment of adoptively transferred ERT2-Cre$^+$ NK cells with necrostatin for 6 d consecutively during tamoxifen-induced A20 deletion did not rescue NK cell death. To definitely exclude a potential role for RIPK3, we employed a complementary genetic approach and generated NK-A20$^{-/-}$ × *RIPK3$^{-/-}$* mice. The loss of RIPK3 on top of A20 did not restore NK cell numbers, showing that A20-

deficient NK cells do not die in a RIPK3-dependent manner (Fig. 3 C). Overall, these data reveal that A20-deficient NK cells die through apoptosis in a RIPK3- and RIPK1-independent manner.

A20-deficient NK cells are more sensitive to TNF

A20 deficiency has been shown before to sensitize hepatocytes and enterocytes to TNF-induced cell death (Vereecke et al., 2010; Catrysse et al., 2016). Although these cell types do not die spontaneously upon loss of A20, widespread apoptosis can be observed upon injection of sublethal doses of TNF or in combination with myeloid-specific loss of A20, which leads to increased serum levels of TNF (Vereecke et al., 2014). Importantly, NK cells express the p55 TNFRI on their cell surface (Fig. S3 A), and a TNF dose titration experiment on ex vivo–cultured splenocytes showed that A20$^{-/-}$ NK cells are also hypersensitive to TNF-induced cytotoxicity (Fig. 3 D). What is the source of TNF? Similar to what we found for IFNγ, NK-A20$^{-/-}$ cells displayed enhanced levels of intracellular TNF at baseline (Fig. S3 B); however, this was not reflected by increased serum TNF levels or enhanced TNF secretion in ex vivo cultures (Fig. S3, C and D). As a positive control, we used serum from A20^{mZnF7} mice (mouse line described in Fig. 5). Still, this did not exclude the possibility that NK cells would be sensitized to TNF secreted by other cell types. To assess the role of TNF in NK cell death, we injected CD45.1 acceptor mice for 6 d consecutively with a TNFα antibody during the treatment with tamoxifen to delete A20 in adoptively transferred ERT2-Cre$^+$ NK cells. As can be seen in Fig. 3 E, concomitant blocking of TNF-mediated signaling pathways partially rescued NK cell death induced by loss of A20. In a complementary genetic approach, we generated compound-deficient NK-A20$^{-/-}$ × *TNF$^{-/-}$* mice. Similar to what we found for the Bcl2$^{Tg/+}$ mice, loss of TNF by itself is sufficient to increase NK cell numbers in the spleen already at baseline (Fig. 3 F). Notably, the rescue of A20-deficient NK cells by compound deficiency of TNF is considerably higher, implementing a TNF-dependent apoptotic pathway in the cell death induced by loss of A20. Still, additional loss of TNF did not restore A20$^{-/-}$ NK cell numbers back to WT NK cell numbers in the spleen, suggesting that A20 acts at multiple levels in the protection against cell death.

A20-deficient NK cells display elevated mTOR activation

As NK cell homeostasis is intricately associated with IL-15 and STAT5 signaling (Cooper et al., 2002; Vosshenrich et al., 2005; Eckelhart et al., 2011), we assessed whether A20 might modulate this pathway. The phosphorylation status of STAT5 was not different between NK-A20$^{-/-}$ and littermate NK cells either in basal conditions or upon stimulation with IL-15, indicating that signaling immediately downstream of the IL-15 receptor was not affected by loss of A20 (Fig. 4 A). Along these lines, the levels of CD122 (IL-2/IL-15 receptor β chain) were unaltered in NK-A20$^{-/-}$ cells (data not shown). Recent data implemented a role for the metabolic checkpoint kinase mTOR in IL-15–dependent signaling (Marçais et al., 2014). Notably, in T cells, mTOR activity was enhanced upon loss of A20 (Matsuzawa et al., 2015). Also, NK-A20$^{-/-}$ cells showed strongly enhanced mTORC1
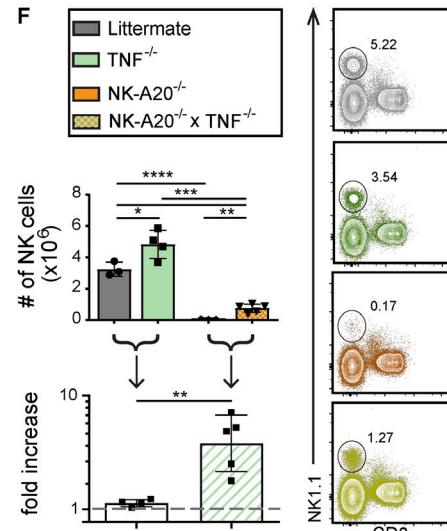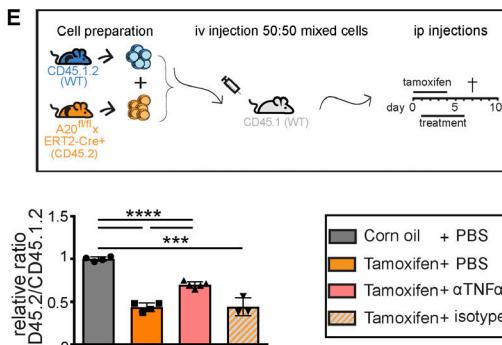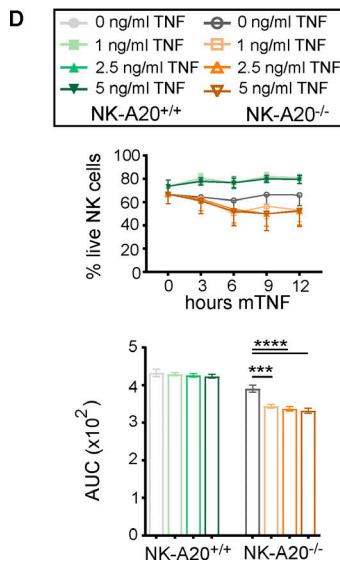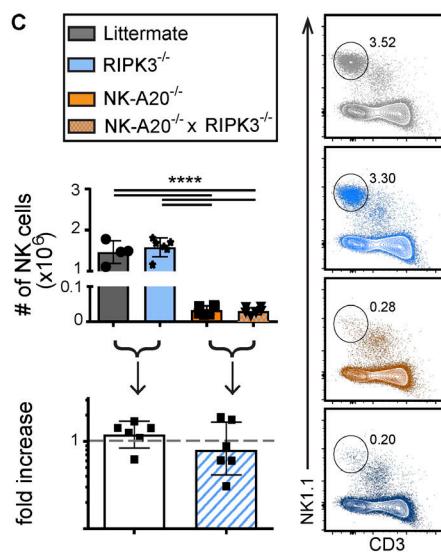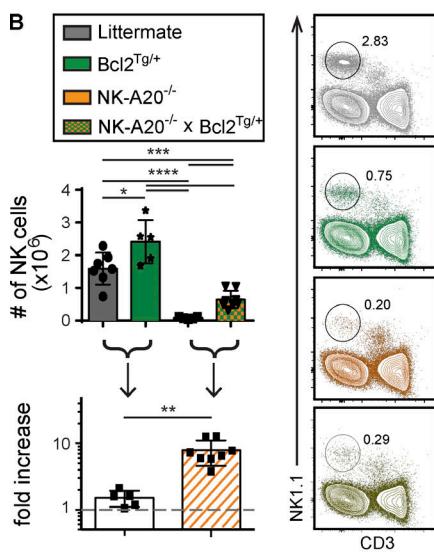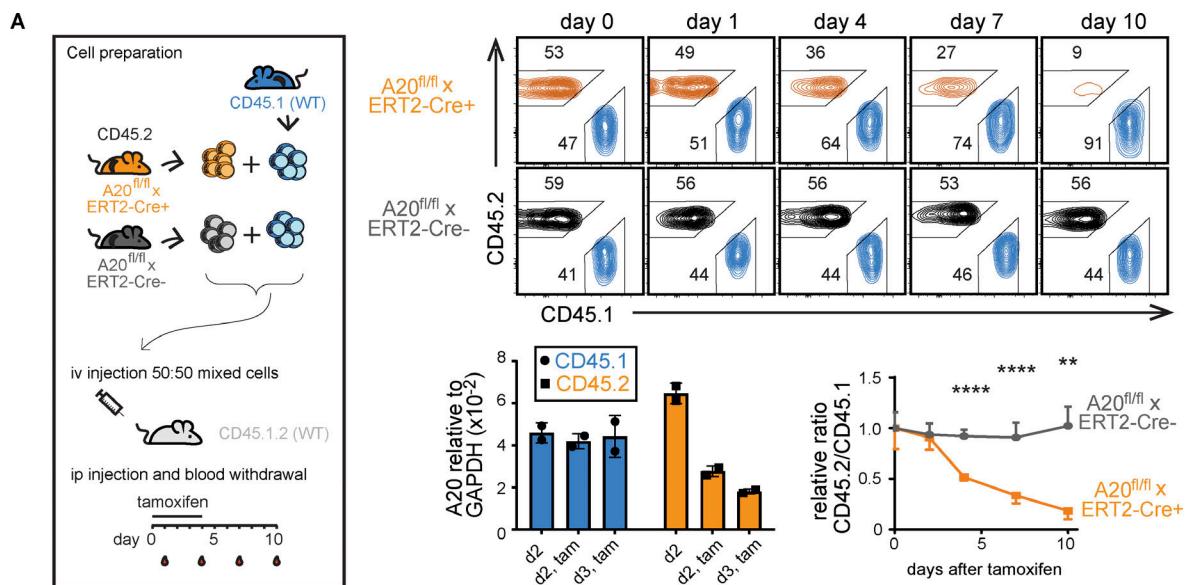
Figure 3.   **A20 is indispensable for NK cell survival. (A)** Graphical representation of adoptive cell transfer setup. FACS plots show the frequency of CD45.1 and CD45.2 donor NK cells, and survival graph shows CD45.2/CD45.1 donor NK cell ratios compared with day 0 as measured over time in the blood. Bar graph depicts normalized A20 RNA expression as determined by RT-qPCR on sorted splenic CD45.1 or CD45.2 donor NK cells upon tamoxifen (tam) or vehicle control treatment. **(B, C, and F)** Flow cytometry analysis on splenic NK cells isolated from indicated mouse lines. Bar graphs represent NK cell absolute numbers and the fold expansion, and FACS plots depict the proportion of NK cells per genotype. **(D)** Freshly isolated NK-A20 splenocytes were subjected to a dose range of mTNF over time. Survival curves (upper graph) represent NK cell viability as assessed by annexin V and live/dead staining on flow cytometry, and bar graphs (lower panel) show AUC for indicated mTNF doses per genotype. For readability, significant differences are shown only per genotype but were also evident between genotypes (****, $P < 0.0001$ per dose). **(E)** Graphical representation of adoptive cell transfer setup with indicated treatments. Bar graphs represent the ratio of donor-derived CD45.2/.1.2 NK cells, relative to the control group, as determined by flow cytometry. All bar graphs represent mean ± SD, and dots represent individual mice. Data are representative of at least two independent experiments, with exceptions of A (RT-qPCR data) and D, which were performed only once. Statistics were performed with unpaired Student's t test: *, $P < 0.05$; **, $P < 0.01$; ***, $P < 0.001$; ****, $P < 0.0001$. For AUC analyses, see Materials and methods.

activity as evidenced by increased phosphorylation of downstream mTOR substrates 4EBP1 and S6, which was particularly prominent in steady state (Fig. 4 A). Also, other targets of mTOR signaling, such as cell surface expression of the transferrin receptor CD71 or the amino acid transporter CD98, were markedly elevated, while ex vivo incubation of splenocytes with the fluorescent glucose analogue 2-NBDG revealed that NK-A20$^{-/-}$ cells displayed increased glucose uptake (Fig. 4 B). In line with these data, NK-A20$^{-/-}$ cells showed increased in vivo protein synthesis, as revealed by O-propargyl puromycin (OP-Puro) incorporation in mixed BM chimeric mice (Fig. 4 C; Signer et al., 2014; Tavernier et al., 2017). Overall, these data indicate that A20 acts as a metabolic checkpoint inhibitor in NK cells.

To assess whether this enhanced mTOR activity was contributing to the observed NK-A20$^{-/-}$ cell death, we injected CD45.1 acceptor mice for 6 d consecutively with rapamycin, an established inhibitor of mTORC1, to see if we could restore tamoxifen-induced cell death of ERT2-Cre$^+$ A20-deficient NK cells. As can be seen in Fig. 4 D (middle panel), we obtained a clear rescue of A20$^{-/-}$ NK cells by damping the exacerbated mTOR signaling by rapamycin, classifying mTOR as a bona fide target in the A20-mediated decision between life and death.

To test whether the TNF and mTOR pathways act independently or belong to one and the same pathway, we concomitantly blocked both TNF and mTOR during the tamoxifen-induced deletion process of A20 and assessed whether the two inhibitors worked synergistically. As can be noted from Fig. 4 D (lower panel), each inhibitor individually rescued part of the NK cells, but together they led to a complete restoration of NK cell death induced by loss of A20. This suggests that both TNF hypersensitivity and exacerbated mTOR signaling contribute separately to NK cell death in conditions of A20 deficiency.

A20 comprises a deubiquitinase domain as well as ubiquitin-binding domains. Our department recently generated a ubiquitous zinc finger 7 (ZnF7) knock-in mouse model for A20, in which cysteine residues 764 and 767 in ZnF7 domain were mutated (referred to as A20^{mZnF7}) to abrogate binding of A20 to linear ubiquitin chains in all cells (Polykratis et al., 2019). A20$^{mZnF7/mZnF7}$ mice suffer from massive hyperinflammation and develop arthritis, similar to mice deficient for A20 in myeloid cells (Polykratis et al., 2019). To elucidate how A20 mediates its homeostatic role in NK cells, we immunophenotyped the splenic NK cell compartment in the A20$^{mZnF7/mZnF7}$ mice and found that impairment of A20 linear ubiquitin binding causes

massive cell death in NK cells (Fig. 5 A). Similar to what was shown in NK-A20$^{-/-}$ mice, mTOR activity was highly elevated in A20$^{mZnF7/mZnF7}$ cells (Fig. 5 B), while intracellular TNF levels in A20$^{mZnF7/mZnF7}$ cells did not differ (Fig. 5 C). However, at the serum level, we found a massive increase in TNF in the A20$^{mZnF7/mZnF7}$ mice (Fig. S3 C).

In summary, we unraveled a cell-intrinsic role for A20 in controlling NK cell survival by acting on the TNFRI and mTOR complexes. Constitutive loss of A20 in NK cells led to severe and widespread NK cell lymphopenia due to NK cell death. Remaining NK cells were hyperactive and hyperproliferative, produced more proinflammatory cytokines, and had increased cytotoxic properties. Despite the well-established anti-apoptotic role of A20 (Lee et al., 2000), NK cells are, to our knowledge, the first cell type that die in a spontaneous manner upon loss of A20. B cells and dendritic cells show strongly enhanced survival, due to the up-regulation of Bcl-2 and Bcl-xL, and are even more resistant to Fas-induced cell death (Tavares et al., 2010; Kool et al., 2011). Strikingly, despite strongly enhanced activation of the NF-κB pathway in NK-A20$^{-/-}$ cells (as monitored by P-p65 levels), antiapoptotic NF-κB–dependent genes were not induced, showing complex regulation of NF-κB transcriptional activity in NK cells. In T cell–specific conditional A20$^{-/-}$ mice, frequency and numbers of CD4$^+$CD8$^+$ double-positive thymocytes, CD8$^+$ or CD4$^+$ single-positive thymocytes, and peripheral T cells were normal (Onizawa et al., 2015). Only upon TCR triggering could marked reductions in T cell numbers be observed, suggesting that A20 was needed to protect activated T cells from dying (Onizawa et al., 2015). Similarly, in hepatocytes and enterocytes, loss A20 did not lead to spontaneous cell death, but rather caused hypersensitivity to sublethal doses of TNF (Vereecke et al., 2010; Catrysse et al., 2016). In NKT cells, A20 controlled survival of NKT1 and NKT2 to some extent, and not NKT17 subsets, but never led to the dramatic cell loss observed for NK-A20$^{-/-}$ cells (Drennan et al., 2016). Loss of A20-deficient NKT cells could be prevented by compound deficiency with MALT1, a proteolytic enzyme in the Carma-Bcl10-Malt1 complex downstream of the TCR and a well-established target of A20. However, this pathway appeared not to be involved in A20-mediated cell death of NK cells (data not shown). Part of the mechanism leading to spontaneous loss of NK cells in the absence of A20 was explained by the hyperactivated state of A20$^{-/-}$ NK cells, which led to increased proinflammatory TNF production, either direct or indirect. Due to the loss of A20 and
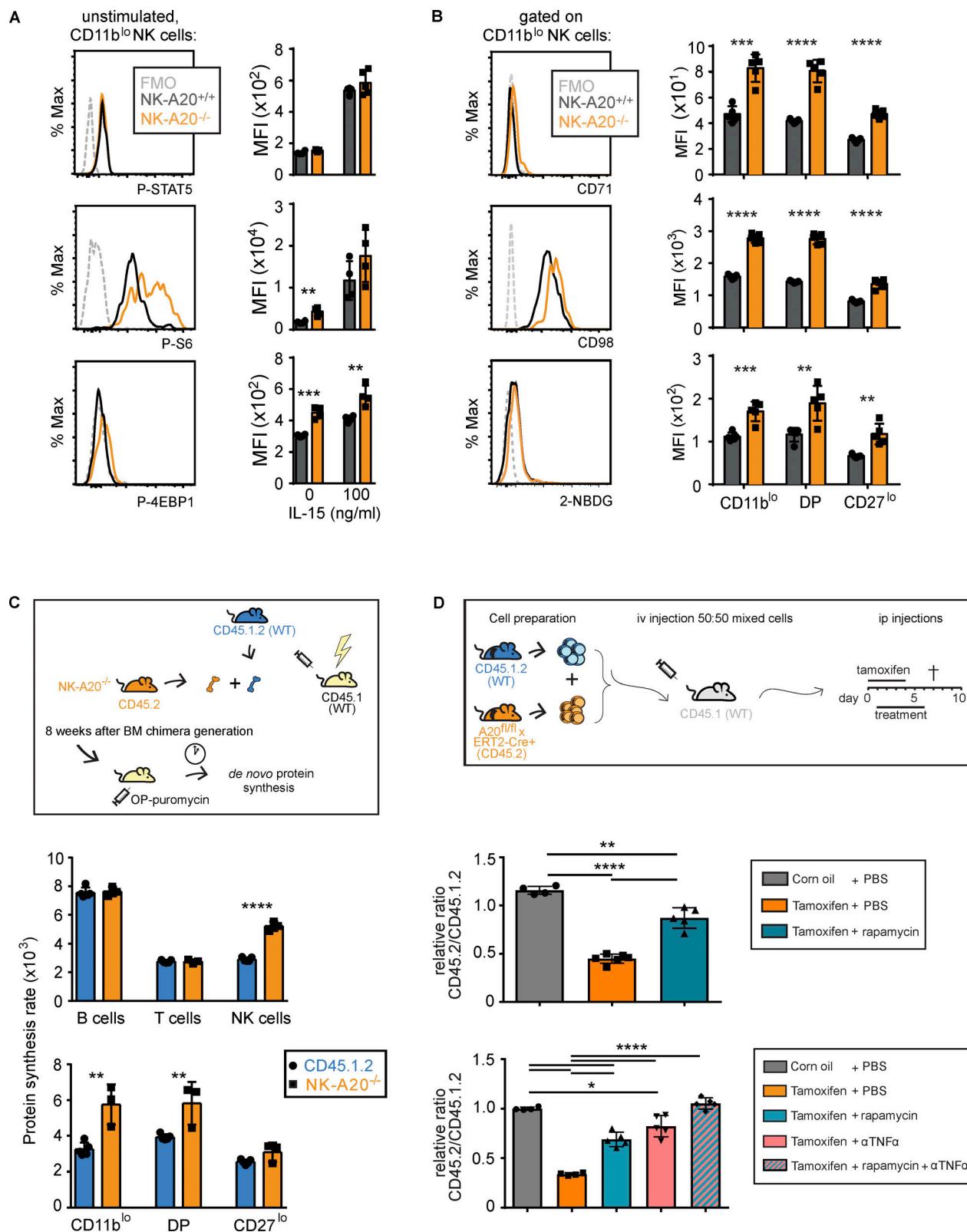
Figure 4. **A20 restricts the metabolic activity of NK cells. (A and B)** Flow cytometry analysis of splenic NK cells isolated from NK-A20 mice. **(A)** Histograms show steady state phosphorylation (p-) of indicated proteins in CD11b^{lo} NK cells measured by phosphoflow. Bar graphs depict mean fluorescence intensity (MFI) of phosphorylated proteins in steady state or upon IL-15 stimulation. FMO, fluorescence minus one. **(B)** Histograms show 2-NBDG uptake and CD71 and CD98 expression as measured on steady state CD11b^{lo} NK cells. Bar graphs depict MFI of the indicated parameters in NK cell subsets. DP, double positive. **(C)** Graphical representation of OP-Puro incorporation in NK-A20 BM chimeras. Bar graphs represent OP-Puro fluorescence as measured by flow cytometry in splenic donor-derived CD45.1.2 (WT) or CD45.2 lymphocyte populations. **(D)** Graphical representation of adoptive cell transfer setup. Bar graphs depict the

ratio of donor-derived CD45.2/.1.2 NK cells, relative to the control group, as determined by flow cytometry. For all figures, bar graphs represent mean ± SD, and dots represent individual mice. Data are representative of at least two independent experiments. Unpaired Student's *t* test: *, P < 0.05; **, P < 0.01; ***, P < 0.001; ****, P < 0.0001.

concomitant hypersensitivity to TNF-induced killing, this caused NK cell death. Still, as was obvious from the compound deficient NK-A20$^{-/-}$ × TNF$^{-/-}$ mice, NK cell numbers could not be restored to WT levels, indicating that additional mechanisms were needed to explain the A20-mediated protection against cell death.

We turned our attention toward the mTOR signaling cascade, a pathway that was recently established as a critical regulator of NK cell homeostasis and considered a hallmark for reactive NK cells (Marçais et al., 2014, 2017). Loss of A20 dramatically increased mTOR signaling output, as monitored by enhanced downstream phosphorylation of 4EBP1 and S6, enhanced glucose uptake, and enhanced translation. This occurred independently of IL-15 receptor signaling, as both IL-15 receptor levels and signaling steps immediately downstream of the IL-15 receptor were unaffected. Rather, we propose that A20 could directly target either mTOR or any of its regulators in the mTOR signaling complex by ubiquitination, as suggested before for T cells (Matsuzawa et al., 2015). It has been shown that increased ubiquitination of mTOR and/or proteins within the mTOR signaling complex are associated with restrained mTOR activity, in an as yet ill-defined manner (Ivanov and Roy, 2013). Indeed, a newly generated A20^{mZnF7} knock-in mouse model confirmed that ZnF7 is absolutely essential for A20 to restrict mTOR activity and preserve NK cell homeostasis, implying a potential role for A20 in stabilization of M1 ubiquitin chains on mTOR or associated proteins.

We can only speculate how increased mTOR signaling causes NK cell death. Activation of mTOR has been associated before with increased NK cell reactivity, resulting in enhanced calcium influxes upon triggering of NK activating receptors (Marçais et al., 2017). Furthermore, increased translation is linked with increased production of oxygen radicals (Han et al., 2013). While not formally proven, it is not difficult to conceive that both calcium overload and ROS production could trigger mitochondrial pathways of cell death. Intriguingly, we observed a robust increase in the expression level of the proapoptotic molecule Noxa in NK-A20$^{-/-}$ cells and found that the cells could be partially rescued by overexpression of Bcl-2, suggesting at least a partial contribution of a mitochondrial pathway of death. Finally, high mTOR activation is also known to interfere with cytoprotective pathways of autophagy. Preliminary data showed that deficiency of Atg16L1, a crucial component of autophagosome formation (Fujita et al., 2008; Adolph et al., 2013), also causes NK cell loss in a dose-dependent manner (data not shown). These data confirm that a tight balance of mTOR signaling and autophagy is crucial for proper NK cell homeostasis (O'Sullivan et al., 2016).

In conclusion, here we established a critical role for A20 in restricting mTOR activity in NK cells, adding a novel player in the decision of A20 between life and death. We postulate that NK cells, being exquisitely sensitive to balances between inhibitory and activating signals, are particularly vulnerable to any dysregulation of these balances and therefore prone to death when a crucial regulator such as A20 is lost.

Materials and methods

Mice
The *Ncr1*$^{iCre/+}$ mouse line was originally described in Narni-Mancinelli et al. (2011); *A20*$^{fl/fl}$ mice in Vereecke et al. (2010); *RIPK3*$^{-/-}$ in Newton et al. (2004); *H2K-bcl-2*$^{tg/+}$ in Domen et al. (1998); *TNF*$^{-/-}$ mice in Pasparakis et al. (1996); and A20^{mZnF7} mice in Polykratis et al. (2019). The *ERT2-Cre*$^{tg/+}$, CD45.1, and CD45.1.2 mice are provided by the Jackson Laboratory. The following mouse lines were bred and housed under specific pathogen–free conditions at the VIB–Ghent University Center for Inflammation Research: *Ncr1*$^{+/+}$ × *A20*$^{fl/fl}$, *Ncr1*$^{iCre/+}$ × *A20*$^{+/fl}$ or *A20*$^{fl/fl}$ (NK-A20$^{+/+}$, NK-A20$^{+/-}$, or NK-A20$^{-/-}$), NK-A20$^{-/-}$ × *RIPK3*$^{-/-}$, NK-A20$^{-/-}$ × *TNF*$^{-/-}$, *A20*$^{fl/fl}$ × *ERT2-Cre*$^{tg/+}$, CD45.1, CD45.1.2, and A20^{mZnF7}. The NK-A20$^{-/-}$ × *H2K-bcl-2*$^{tg/+}$ mouse line was housed at the Campus Proeftuinstraat Ghent University site. All transgenic mouse lines have been generated on a C57Bl/6 background (*Ncr1*$^{iCre/+}$, *A20*$^{fl/fl}$, *ERT2-Cre*$^{tg/+}$, and A20^{mZnF7}) or were backcrossed for >10 generations to C57Bl/6 (*H2K-bcl-2*$^{tg/+}$, *RIPK3*$^{-/-}$, *TNF*$^{-/-}$ transgenic mice). All experiments with the NK-A20 mice were performed with NK-A20$^{+/+}$ animals as littermate controls. In the case of adoptive transfers or BM chimeras, CD45.1/2 congenically marked animals were included as WT counterparts. All animal experiments were performed in accordance with institutional guidelines for animal care of the VIB site Ghent/Ghent University Faculty of Sciences and in accordance with ethical committee EC2014_043. Litters with mice of both sexes at 6–17 wk of age were used for experiments.

Generation of BM chimeras
CD45.1 recipient mice received two rounds of sublethal irradiation (400 cG) with a time interval of 4 h. At least 4 h after the second irradiation cycle, recipient mice were injected intravenously with a 50:50 mixture of BM cells (either 2 × 10^6 or 4 × 10^6) derived from CD45.1.2 and NK-A20$^{+/+}$, NK-A20$^{+/-}$, or NK-A20$^{-/-}$ donors. Mice were used for experiments ≥8 wk after reconstitution.

Preparation of single-cell suspensions
For all figures except Fig. S1, spleens and mediastinal lymph nodes were smashed over a 70-µM filter, and red blood cells were removed from the spleen by osmotic lysis. For Fig. S1, an enzymatic digestion protocol was followed that ensures proper isolation of the myeloid compartment. Spleens were first minced, digested for 30 min in RPMI 1640 (Gibco) containing Liberase TM (0.02 mg/ml; Roche) and DNase I (10 U/ml; Roche) in a shaking water bath at 37°C, filtered through a 70-µM filter, and subjected to osmotic lysis. For BM, single-cell suspensions

Figure 5. **A20 controls NK cell survival and the mTOR pathway through its ZnF7 domain. (A–C)** Flow cytometry analysis of steady state splenic NK cells isolated from indicated mouse lines. **(A)** Bar graphs depict NK cell absolute numbers. **(B)** Histograms and bar graphs depict MFI of the indicated phosphorylated proteins as determined by phosphoflow. **(C)** Bar graphs show TNF MFI in total NK cells (no prior stimulation). All bar graphs represent mean ± SD, and dots show individual mice. All data are representative of at least two independent experiments, and statistical analysis was performed with a one-way ANOVA (ad hoc Tukey's multiple comparisons test). *, $P < 0.05$; **, $P < 0.01$; ***, $P < 0.001$; ****, $P < 0.0001$. **(D)** Model depicting the possible role of A20 in NK cells. Upper panel: Through its Zn fingers, A20 binds and stabilizes M1-linked ubiquitin chains in the TNF receptor complex. As such, A20 competes with NF-κB essential modulator (NEMO) for binding to key components in the receptor disc and thereby interferes with NF-κB activation. At the same time, by stabilizing M1 ubiquitin chains, A20 also prevents the deubiquitinase cylindromatosis (CYLD) from degrading linear ubiquitin chains. This precludes formation of the proapoptotic complex II. Lower panel: Loss of A20 leads to strongly enhanced NF-κB activation and release of cytokines, such as TNF, in either a direct or indirect manner. Due to the enhanced sensitivity to TNF-mediated killing in the absence of A20, NK cells die. Additionally, A20 also restricts mTOR activity in NK cells, preventing spontaneous hyperactivation of this pathway. Loss of A20 leads to mTOR overactivation and mTOR-dependent NK cell death, which could be due to enhanced translation and increased production of ROS, to a block in autophagy and/or other signaling pathways. LUBAC, linear ubiquitination assembly complex.

were obtained by crushing the tibia and femur, followed by lysis of red blood cells. In the case of lung and liver, organs were collected from PBS-perfused mice, minced, and digested at 37°C for 20–45 min in RPMI 1640 (Gibco) containing DNase I (10 U/ml; Roche) and collagenase A (1 mg/ml; Sigma-Aldrich). Lungs required a single GentleMACS dissociation step (after digestion), while livers were subjected to two rounds of GentleMACS

dissociation (before and after digestion). Red blood cells were removed by osmotic lysis, and an additional Percoll-gradient centrifugation step was performed for the liver. To isolate cells from the lamina propria, the small intestine was dissected, Peyer's patches were removed, and the intestine was opened longitudinally and then minced using scissors. Epithelial cells were removed by serial washes at 37°C with HBSS without Ca²⁺

and Mg^{2+} (Gibco) containing 10% FCS (Bodinco) and 2 mM EDTA (Lonza). The lamina propria was subsequently digested at 37°C for 15–20 min in RPMI 1640 supplemented with 10% FCS, collagenase A (0.24 mg/ml; Sigma-Aldrich) and DNase I (50 U/ml; Roche), followed by Percoll-gradient centrifugation. Tail vein blood was collected in Microvette 200 K3E tubes (Sarstedt), and red blood cells were cleared by several rounds of osmotic lysis. Serum samples were obtained from femoral artery (terminal) bleeding. Blood was collected in Eppendorf tubes and stored at room temperature for ≥2–3 h. Samples were then centrifuged for 10 min at 5,000 rpm, and supernatant was collected and stored at −20°C.

Flow cytometry and gating strategy

Single-cell suspensions were obtained as described and stained with monoclonal antibodies labeled with fluorochromes or biotin, recognizing the following markers: activated caspase 3 (C92-605), CD3 (17A2 or 145-2c11), CD11b (M1/70), CD11c (N418), CD16/32 (2.4G2), CD19 (1D3), CD27 (LG.7F9 or LG.3A10), CD45 (30-F11), CD45.1 (A20), CD45.2 (104), CD49a (Ha31/8), CD49b (DX5), CD64 (X54-5/7.1), CD71 (R17217), CD98 (RL388), CD107a (1DB4), CD122 (TM-b1), F4/80 (BM8), IA-IE (M5/114.15.2), IFNγ (XMG1.2), Ki-67 (B56), NK1.1 (PK136), NKp46 (29A1.4), P-4EBP1 (236B4), P-AKT (M89-61), PDCA1 (JF05-1C2.4.1), P-p65 (93H1), P-S6K (D57.2.2E), P-STAT5 (47), Rorγt (AFKJS-9), SiglecF (E50-2440), TCRβ (H57-597), TCRγδ (eBioGL3), and TNF (MP6-XT22). Intracellular stainings for TNF and OP-Puro were performed with the Foxp3 kit (eBioscience). Lyse/Fix and PermIII buffers (BD) were used for intracellular stainings of phosphorylated proteins. Intracellular IFNγ, caspase 3, and Ki-67 stainings were performed with Cytofix/Cytoperm (BD) and Perm/Wash (BD). Cell viability was measured using annexin V (BD) and/or a fixable viability dye (eBioscience). Flow cytometry was performed on a FACS Fortessa 4 or 5 laser (BD Biosciences), and data were analyzed using FlowJo.

The following gating strategy was applied for NK-A20 immunophenotyping: B cells (live, CD3$^-$CD19$^+$), T cells (live, CD19$^-$NK1.1$^-$CD3$^+$), CD4$^+$ T cells (live, CD19$^-$NK1.1$^-$CD3$^+$TCRγδ$^-$CD4$^+$), CD8$^+$ T cells (live, CD19$^-$NK1.1$^-$CD3$^+$TCRγδ$^-$CD8$^+$), macrophages (live, CD19$^-$NK1.1$^-$CD3$^-$F4/80$^+$CD64$^+$ autofluorescent), dendritic cells (live, CD19$^-$NK1.1$^-$CD3$^-$ [not macrophages] CD11c$^+$MHCII$^+$), NK cells (live, CD19$^-$CD3$^-$NK1.1$^+$), NK T cells (live, CD19$^-$CD3$^+$NK1.1$^+$), neutrophils (live, CD19$^-$NK1.1$^-$CD3$^-$ [not basophils] CD11b$^+$Ly6G$^+$), eosinophils (live, CD19$^-$NK1.1$^-$CD3$^-$ [not basophils or neutrophils] CD11c$^-$SiglecF$^+$SSC^{hi}), Ly6C^{hi} monocytes (live, CD19$^-$NK1.1$^-$CD3$^-$ [not basophils, neutrophils, or eosinophils] CD11b$^+$Ly6C$^+$), plasmacytoid dendritic cells (live, CD19$^-$NK1.1$^-$CD3$^-$ [not basophils, neutrophils, eosinophils, or Ly6C^{hi} monocytes] Ly6C$^+$PDCA1$^+$), and γδ T cells (live, CD19$^-$NK1.1$^-$CD3$^+$TCRγδ$^+$). The following standard gating strategy was used for NK cells throughout the article: live, CD19$^-$CD3$^-$NK1.1$^+$CD122$^+$CD49b$^+$. In FACS plots showing NK cells, numbers depict frequencies of NK cells of total live cells. Depending on antibody availability, CD122$^+$ was sometimes replaced by NKp46$^+$, and CD19 was not always added. For phosphoflow, the following NK cell gating was applied: live, CD3$^-$NK1.1$^+$NKp46$^+$, or live, CD3$^-$NK1.1$^+$CD49b$^+$. For some stainings, fluorescence minus one was used as a control.

Cell sorting and gating strategy

Leukocytes were obtained from the spleen as described and, before sorting, enriched for NK cells with the MagniSort NK cell enrichment kit (eBioscience) or with an in-house optimized enrichment procedure using MACS columns (negative selection with stainings against CD5, CD24, TCRβ, CD19, F4/80, CD3, Ter119, and Ly6G). For sorting T, B, and NK cells, the obtained single-cell suspension was divided in two fractions. One fraction was immediately stained for T and B cells, and the second fraction was used for NK enrichment before staining. Up to 40,000 cells (T, B, and NK cells) were sorted directly in RLT Plus Buffer (RNeasy plus micro kit; Qiagen) supplemented with β-mercaptoethanol (10 μl/ml). Samples were snap frozen and stored at −80°C until further processing. Cell sorting was performed on a FACS AriaII and III (BD Biosciences). The following gating strategies were applied: B cells (live, CD19$^+$), T cells (live, CD19$^-$NK1.1$^-$CD3$^+$), and NK cells (live, CD3$^-$TCRβ$^-$CD19$^-$CD122$^+$NK1.1$^+$CD49b$^+$, or live, CD3$^-$CD19$^-$TCRβ$^-$NK1.1$^+$NKp46$^+$).

RNA extraction and quantitative RT-PCR (RT-qPCR)

RNA from sorted cells was obtained using the RNEasy Plus Micro Kit (Qiagen) according to the manufacturer's instructions. cDNA was generated with the SensiFAST cDNA Synthesis Kit (Bioline) or the iScript cDNA synthesis kit (Bio-Rad Laboratories) or amplified with the Ovation PicoSL WTA System V2 kit (NuGEN) following the manufacturer's guidelines. Upon amplification, pollutants were removed using the MinElute PCR purification kit (Qiagen) before SybrGreen-based RT-qPCR with the SensiFast SYBR No-ROX kit (Bioline) on a LightCycler 480 (Roche). The following mouse primers were used: A20, forward 5′-AAACCAATGGTGATGGAAACTG-3′ and reverse 5′-GTTGTCCCATTCGTCATTCC-3′; β-actin, forward 5′-GCTTCTAGGCGGACTGTTACTGA-3′ and reverse 5′-GCCATGCCAATGTTGTCTCTTAT-3′; Bcl-2, forward 5′-GTACCTGAACCGGCATCTG-3′ and reverse 5′-GGGGCCATATAGTTCCACAA-3′; Bcl-xL, forward 5′-GACAAGGAGATGCAGGTATTGG-3′ and reverse 5′-TCCCGTAGAGATCCACAAAAGT-3′; Bim, forward 5′-CCCGGAGATACGGATTGCAC-3′ and reverse 5′-GCCTCGCGGTAATCATTTGC-3′; cIAP, forward 5′-TACGGATGAAGGGTCAGGAGT-3′ and reverse 5′-GCACCACTGTCTCTGTAGGG-3′; GAPDH, forward 5′-GCATGGCCTTCCGTGTTC-3′ and reverse 5′-TGTCATCATACTTGGCAGGTTTCT-3′; HPRT, forward 5′-TGAAGAGCTACTGTAATGATCAGTCAAC-3′ and reverse 5′-AGCAAGCTTGCAACCTTAACCA-3′; Mcl-1, forward 5′-CAAAGATGGCGTAACAAACTGG-3′ and reverse 5′-CCGTTTCGTCCTTACAAGAACA-3′; Noxa, forward 5′-ACTGTGGTTCTGGCGCAGAT-3′ and reverse 5′-TTGAGCACACTCGTCCTTCAA-3′; Puma, forward 5′-ATGGCGGACGACCTCAAC-3′ and reverse 5′-GGAGTCCCATGAAGAGAT-3′; and XIAP, forward 5′-GTGGTACCCAGGGTGCAAATA-3′ and reverse 5′-TGCTCCCGGATGTTTGGATT-3′. mRNA expression levels were analyzed using qBAse+ software (Biogazelle).

Cell culture and stimulation

For the measurement of IFNγ production and degranulation, 3 × 10^6 splenocytes were cultured in RPMI 1640 (Gibco) supplemented with 10% FCS (Bodinco) in the presence of GolgiStop (BD) and anti-CD107a (BD). The cells were cultured in the

presence of cytokines (rmIL-12 at 25 ng/ml [Peprotech], rmIL-18 at 5 ng/ml [Peprotech], and rmIL-2 at 20 ng/ml [Protein Service Facility, VIB]) or were cultured on antibody-coated plates (anti-NK1.1 at 10 µg/ml) for 4 h at 37°C. For p-4EBP1 and p-S6 phosphoflow, 4×10^6 splenocytes were stimulated for 1 h at 37°C in the presence or absence of rmIL-15 (100 ng/ml; Peprotech), after which cell surface stainings were performed as described, followed by fixation and intracellular stainings. For steady state and stimulation-induced P-p65 phosphoflow, 3×10^6 splenocytes were either stained immediately ex vivo or stimulated for 5 or 15 min at 37°C with 1 or 10 ng/ml mouse TNF (mTNF; Tissue Culture Core, VIB). Untreated cells were used as controls at these time points. Culture medium for phosphoflow experiments consisted of RPMI 1640 supplemented with 10% FCS. For TNF hypersensitivity, 2×10^6 splenocytes were cultured for 0, 3, 6, 9, and 12 h at 37°C in tissue culture medium (RPMI 1640, 10% FCS, Glutamax [Life Technologies], Gentamicin [Gibco], and β-mercaptoethanol [Tissue Culture Core, VIB]) and supplemented with 0, 1, 2.5, or 5 ng/ml mTNF. 9- and 12-h cultures were supplemented with low-dose rmIL-15 (10 ng/ml; Peprotech). Cell viability was determined by annexin V and live/dead staining, as described. For glucose uptake, 2×10^6 splenocytes were incubated for 10 min in RPMI 1640 supplemented with 100 µM of the fluorescent glucose analogue 2-NBDG (Thermo Fisher Scientific) before staining of cell surface proteins as described. For ELISA, 10^6 splenocytes or enriched splenic NK cells were cultured for 24 h in tissue culture medium. After 24 h, supernatant was collected and stored at –20°C.

ELISA
TNF secretion was determined by ELISA (eBioscience) following the manufacturer's guidelines. Samples included serum or supernatant from 24-h–cultured enriched NK cells or splenocytes. See Preparation of single-cell suspensions and Cell culture and stimulations for further details.

Adoptive cell transfers
NK cells were isolated and enriched from the spleens of CD45.1 (WT) or CD45.1.2 (WT) and A20$^{fl/fl}$ × ERT2-Cre$^-$ or Cre$^+$ animals, and a 1:1 mixture of donor cells (total number of cells: $4–5 \times 10^5$) was given i.v. to congenic recipients. Immediately after cell transfer, recipient mice were treated with tamoxifen (or corn oil as control) for 5 d, and in some cases also with indicated chemical compounds for 6 d consecutively, unless stated otherwise. The ratio of donor NK cells in the blood or spleen of the recipient animals was determined by flow cytometry. For validation of the tamoxifen-inducible ablation of A20, donor NK cells were sorted from the spleens of recipients after 2- or 3-d tamoxifen treatment, and A20 expression was determined by RT-qPCR.

Chemical compounds
Tamoxifen (Sigma-Aldrich) was dissolved in corn oil (20 mg/ml; Sigma-Aldrich) and injected i.p. (2 mg/mouse) for 5 d, unless stated otherwise. Corn oil (Sigma-Aldrich) was used as vehicle control. Nec1s (100 mM in DMSO; kindly donated by N. Takahashi) was injected i.v. (6.25 mg/kg) after further dilution in

endotoxin-free PBS (Gibco) to reach a final DMSO content of 2.5%. Rapamycin (InvivoGen) was dissolved in DMSO (10 mM), diluted in endotoxin-free PBS (Gibco), and injected i.p. (0.6 mg/kg) at a final DMSO content of 1%. TNFα (2.6 mg/ml; clone XT22; Bioceros) and isotype control (rat IgG1; clone GL113; 1.9 mg/ml; Bioceros) were diluted in endotoxin-free PBS (Gibco) and injected i.p. (10 mg/kg). Treatment with one of the above compounds started 1 d after the start of the tamoxifen treatment and lasted 6 d.

Measurement of protein synthesis
OP-Puro (Jena Bioscience) was dissolved in DMSO, further diluted in endotoxin-free PBS (50 mg/ml; Gibco), and injected i.p. (50 mg/kg). 1 h after injection, mice were euthanized, and lymphocytes were obtained from the spleens as described above. 5×10^6 cells were stained for surface markers and subsequently fixed and permeabilized using the Foxp3 kit (eBioscience). For OP-Puro labeling, Alexa Fluor 647 picolyl azide (AF647 PCA; Thermo Fisher Scientific) was chemically linked to OP-Puro through a copper-catalyzed azide-alkyne cycloaddition. In short, 0.5 µM AF647 PCA was dissolved in the Click-iT Cell Reaction Buffer (Thermo Fisher Scientific) containing 200 µM $CuSO_4$. Immediately after preparation, cells were incubated with this mixture at room temperature. After 10-min incubation, the reaction was quenched by addition of PBS supplemented with 5% FCS (Bodinco) and 5 mM EDTA (Lonza). Cells were washed twice to remove unbound AF647 PCA.

Statistical analyses
Datasets were analyzed with two-tailed unpaired Student's t test, Mann–Whitney U test (i.e., nonparametric analogue of Student's t test), or one-way ANOVA combined with Tukey's multiple comparisons test. For TNF hypersensitivity, we performed area under the curve (AUC) analysis on normalized data, determined by the ratio of live cells at a given time point (3, 6, 9, or 12 h) to live cells at the start of the experiment (0 h). Ratios were determined per biological replicate per dose. Ad hoc unpaired Student's t tests were performed on average normalized AUC data per dose per genotype. All statistical tests were performed with Prism (GraphPad Software), and P values express the levels of significance (*, $P < 0.05$; **, $P < 0.01$; ***, $P < 0.001$; ****, $P < 0,0001$). Error bars represent the SD.

Online supplemental material
Fig. S1 shows the immunophenotyping of different immune cell populations in spleen, liver, and LP-SI of NK-A20 mice. Fig. S2 shows an overview of apoptotic markers in A20-deficient NK cells and the effect of necroptosis inhibition in an adoptive transfer setting. Fig. S3 describes TNF levels in A20-deficient NK cells and A20- and TNF compound–deficient NK cells in addition to TNF levels in serum and in ex vivo–cultured splenocytes in different A20 mutant mouse lines.

Acknowledgments

References

Adolph, T.E., M.F. Tomczak, L. Niederreiter, H.-J. Ko, J. Böck, E. Martinez-Naves, J.N. Glickman, M. Tschurtschenthaler, J. Hartwig, S. Hosomi, et al. 2013. Paneth cells as a site of origin for intestinal inflammation. Nature. 503:272–276. https://doi.org/10.1038/nature12599

Alter, G., J.M. Malenfant, and M. Altfeld. 2004. CD107a as a functional marker for the identification of natural killer cell activity. J. Immunol. Methods. 294:15–22. https://doi.org/10.1016/j.jim.2004.08.008

Catrysse, L., L. Vereecke, R. Beyaert, and G. van Loo. 2014. A20 in inflammation and autoimmunity. Trends Immunol. 35:22–31. https://doi.org/10.1016/j.it.2013.10.005

Catrysse, L., M. Farhang Ghahremani, L. Vereecke, S.A. Youssef, C. Mc Guire, M. Sze, A. Weber, M. Heikenwalder, A. de Bruin, R. Beyaert, and G. van Loo. 2016. A20 prevents chronic liver inflammation and cancer by protecting hepatocytes from death. Cell Death Dis. 7:e2250. https://doi.org/10.1038/cddis.2016.154

Chiossone, L., J. Chaix, N. Fuseri, C. Roth, E. Vivier, and T. Walzer. 2009. Maturation of mouse NK cells is a 4-stage developmental program. Blood. 113:5488–5496. https://doi.org/10.1182/blood-2008-10-187179

Chu, Y., J.C. Vahl, D. Kumar, K. Heger, A. Bertossi, E. Wójtowicz, V. Soberon, D. Schenten, B. Mack, M. Reutelshöfer, et al. 2011. B cells lacking the tumor suppressor TNFAIP3/A20 display impaired differentiation and hyperactivation and cause inflammation and autoimmunity in aged mice. Blood. 117:2227–2236. https://doi.org/10.1182/blood-2010-09-306019

Cooper, M.A., J.E. Bush, T.A. Fehniger, J.B. VanDeusen, R.E. Waite, Y. Liu, H.L. Aguila, and M.A. Caligiuri. 2002. In vivo evidence for a dependence on interleukin 15 for survival of natural killer cells. Blood. 100:3633–3638. https://doi.org/10.1182/blood-2001-12-0293

Degterev, A., J. Hitomi, M. Germscheid, I.L. Ch'en, O. Korkina, X. Teng, D. Abbott, G.D. Cuny, C. Yuan, G. Wagner, et al. 2008. Identification of RIP1 kinase as a specific cellular target of necrostatins. Nat. Chem. Biol. 4:313–321. https://doi.org/10.1038/nchembio.83

Domen, J., K.L. Gandy, and I.L. Weissman. 1998. Systemic overexpression of BCL-2 in the hematopoietic system protects transgenic mice from the consequences of lethal irradiation. Blood. 91:2272–2282.

Domen, J., S.H. Cheshier, and I.L. Weissman. 2000. The role of apoptosis in the regulation of hematopoietic stem cells: Overexpression of Bcl-2 increases both their number and repopulation potential. J. Exp. Med. 191:253–264. https://doi.org/10.1084/jem.191.2.253

Drennan, M.B., S. Govindarajan, E. Verheugen, J.M. Coquet, J. Staal, C. McGuire, T. Taghon, G. Leclercq, R. Beyaert, G. van Loo, et al. 2016. NKT sublineage specification and survival requires the ubiquitin-modifying enzyme TNFAIP3/A20. J. Exp. Med. 213:1973–1981. https://doi.org/10.1084/jem.20151065

Eckelhart, E., W. Warsch, E. Zebedin, O. Simma, D. Stoiber, T. Kolbe, T. Rülicke, M. Mueller, E. Casanova, and V. Sexl. 2011. A novel Ncr1-Cre mouse reveals the essential role of STAT5 for NK-cell survival and development. Blood. 117:1565–1573. https://doi.org/10.1182/blood-2010-06-291633

Fujita, N., T. Itoh, H. Omori, M. Fukuda, T. Noda, and T. Yoshimori. 2008. The Atg16L complex specifies the site of LC3 lipidation for membrane biogenesis in autophagy. Mol. Biol. Cell. 19:2092–2100. https://doi.org/10.1091/mbc.e07-12-1257

Han, J., S.-H. Back, J. Hur, Y.-H. Lin, R. Gildersleeve, J. Shan, C.L. Yuan, D. Krokowski, S. Wang, M. Hatzoglou, et al. 2013. ER-stress-induced transcriptional regulation increases protein synthesis leading to cell death. Nat. Cell Biol. 15:481–490. https://doi.org/10.1038/ncb2738

Hayakawa, Y., and M.J. Smyth. 2006. CD27 dissects mature NK cells into two subsets with distinct responsiveness and migratory capacity. J. Immunol. 176:1517–1524. https://doi.org/10.4049/jimmunol.176.3.1517

Huntington, N.D., H. Puthalakath, P. Gunn, E. Naik, E.M. Michalak, M.J. Smyth, H. Tabarias, M.A. Degli-Esposti, G. Dewson, S.N. Willis, et al. 2007. Interleukin 15-mediated survival of natural killer cells is determined by interactions among Bim, Noxa and Mcl-1. Nat. Immunol. 8:856–863. https://doi.org/10.1038/ni1487

Ivanov, S.S., and C.R. Roy. 2013. Pathogen signatures activate a ubiquitination pathway that modulates the function of the metabolic checkpoint kinase mTOR. Nat. Immunol. 14:1219–1228. https://doi.org/10.1038/ni.2740

Kim, S., K. Iizuka, H.-S.P. Kang, A. Dokun, A.R. French, S. Greco, and W.M. Yokoyama. 2002. In vivo developmental stages in murine natural killer cell maturation. Nat. Immunol. 3:523–528. https://doi.org/10.1038/ni796

Kool, M., G. van Loo, W. Waelput, S. De Prijck, F. Muskens, M. Sze, J. van Praet, F. Branco-Madeira, S. Janssens, B. Reizis, et al. 2011. The ubiquitin-editing protein A20 prevents dendritic cell activation, recognition of apoptotic cells, and systemic autoimmunity. Immunity. 35:82–96. https://doi.org/10.1016/j.immuni.2011.05.013

Lee, E.G., D.L. Boone, S. Chai, S.L. Libby, M. Chien, J.P. Lodolce, and A. Ma. 2000. Failure to regulate TNF-induced NF-kappaB and cell death responses in A20-deficient mice. Science. 289:2350–2354. https://doi.org/10.1126/science.289.5488.2350

Marçais, A., J. Cherfils-Vicini, C. Viant, S. Degouve, S. Viel, A. Fenis, J. Rabilloud, K. Mayol, A. Tavares, J. Bienvenu, et al. 2014. The metabolic checkpoint kinase mTOR is essential for IL-15 signaling during the development and activation of NK cells. Nat. Immunol. 15:749–757. https://doi.org/10.1038/ni.2936

Marçais, A., M. Marotel, S. Degouve, A. Koenig, S. Fauteux-Daniel, A. Drouillard, H. Schlums, S. Viel, L. Besson, O. Allatif, et al. 2017. High mTOR activity is a hallmark of reactive natural killer cells and amplifies early signaling through activating receptors. eLife. 6:e26423. https://doi.org/10.7554/eLife.26423

Matsuzawa, Y., S. Oshima, M. Takahara, C. Maeyashiki, Y. Nemoto, M. Kobayashi, Y. Nibe, K. Nozaki, T. Nagaishi, R. Okamoto, et al. 2015. TNFAIP3 promotes survival of CD4 T cells by restricting MTOR and promoting autophagy. Autophagy. 11:1052–1062. https://doi.org/10.1080/15548627.2015.1055494

Minagawa, M., H. Watanabe, C. Miyaji, K. Tomiyama, H. Shimura, A. Ito, M. Ito, J. Domen, I.L. Weissman, and K. Kawai. 2002. Enforced expression of Bcl-2 restores the number of NK cells, but does not rescue the impaired development of NKT cells or intraepithelial lymphocytes, in IL-2/IL-15 receptor beta-chain-deficient mice. J. Immunol. 169:4153–4160. https://doi.org/10.4049/jimmunol.169.8.4153

Vetters et al.
A20 controls NK homeostasis through mTOR and TNF

Journal of Experimental Medicine
https://doi.org/10.1084/jem.20182164

2022

Narni-Mancinelli, E., J. Chaix, A. Fenis, Y.M. Kerdiles, N. Yessaad, A. Reynders, C. Gregoire, H. Luche, S. Ugolini, E. Tomasello, et al. 2011. Fate mapping analysis of lymphoid cells expressing the NKp46 cell surface receptor. *Proc. Natl. Acad. Sci. USA.* 108:18324–18329. https://doi.org/10.1073/pnas.1112064108

Newton, K., X. Sun, and V.M. Dixit. 2004. Kinase RIP3 is dispensable for normal NF-κBs, signaling by the B-cell and T-cell receptors, tumor necrosis factor receptor 1, and toll-like receptors 2 and 4. *Mol. Cell. Biol.* 24:1464–1469. https://doi.org/10.1128/MCB.24.4.1464-1469.2004

Onizawa, M., S. Oshima, U. Schulze-Topphoff, J.A. Oses-Prieto, T. Lu, R. Tavares, T. Prodhomme, B. Duong, M.I. Whang, R. Advincula, et al. 2015. The ubiquitin-modifying enzyme A20 restricts ubiquitination of the kinase RIPK3 and protects cells from necroptosis. *Nat. Immunol.* 16:618–627. https://doi.org/10.1038/ni.3172

Opipari, A.W. Jr., H.M. Hu, R. Yabkowitz, and V.M. Dixit. 1992. The A20 zinc finger protein protects cells from tumor necrosis factor cytotoxicity. *J. Biol. Chem.* 267:12424–12427.

O'Sullivan, T.E., C.D. Geary, O.E. Weizman, T.L. Geiger, M. Rapp, G.W. Dorn 2nd., M. Overholtzer, and J.C. Sun. 2016. Atg5 is essential for the development and survival of innate lymphocytes. *Cell Rep.* 15:1910–1919. https://doi.org/10.1016/j.celrep.2016.04.082

Pasparakis, M., L. Alexopoulou, V. Episkopou, and G. Kollias. 1996. Immune and inflammatory responses in TNF alpha-deficient mice: a critical requirement for TNF alpha in the formation of primary B cell follicles, follicular dendritic cell networks and germinal centers, and in the maturation of the humoral immune response. *J. Exp. Med.* 184:1397–1411. https://doi.org/10.1084/jem.184.4.1397

Polykratis, A., A. Martens, R.O. Eren, Y. Shirasaki, M. Yamagishi, Y. Yamaguchi, S. Uemura, M. Miura, B. Holzmann, G. Kollias, et al. 2019. A20 prevents inflammasome-dependent arthritis by inhibiting macrophage necroptosis through its ZnF7 ubiquitin-binding domain. *Nat. Cell Biol.* 21:731–742. https://doi.org/10.1038/s41556-019-0324-3

Raulet, D.H., and N. Guerra. 2009. Oncogenic stress sensed by the immune system: role of natural killer cell receptors. *Nat. Rev. Immunol.* 9:568–580. https://doi.org/10.1038/nri2604

Renner, F., and M.L. Schmitz. 2009. Autoregulatory feedback loops terminating the NF-kappaB response. *Trends Biochem. Sci.* 34:128–135. https://doi.org/10.1016/j.tibs.2008.12.003

Sathe, P., R.B. Delconte, F. Souza-Fonseca-Guimaraes, C. Seillet, M. Chopin, C.J. Vandenberg, L.C. Rankin, L.A. Mielke, I. Vikstrom, T.B. Kolesnik, et al. 2014. Innate immunodeficiency following genetic ablation of Mcl1 in natural killer cells. *Nat. Commun.* 5:4539. https://doi.org/10.1038/ncomms5539

Signer, R.A.J., J.A. Magee, A. Salic, and S.J. Morrison. 2014. Haematopoietic stem cells require a highly regulated protein synthesis rate. *Nature.* 509:49–54. https://doi.org/10.1038/nature13035

Tavares, R.M., E.E. Turer, C.L. Liu, R. Advincula, P. Scapini, L. Rhee, J. Barrera, C.A. Lowell, P.J. Utz, B.A. Malynn, and A. Ma. 2010. The ubiquitin modifying enzyme A20 restricts B cell survival and prevents autoimmunity. *Immunity.* 33:181–191. https://doi.org/10.1016/j.immuni.2010.07.017

Tavernier, S.J., F. Osorio, L. Vandersarren, J. Vetters, N. Vanlangenakker, G. Van Isterdael, K. Vergote, R. De Rycke, E. Parthoens, L. van de Laar, et al. 2017. Regulated IRE1-dependent mRNA decay sets the threshold for dendritic cell survival. *Nat. Cell Biol.* 19:698–710. https://doi.org/10.1038/ncb3518

Vereecke, L., M. Sze, C. Mc Guire, B. Rogiers, Y. Chu, M. Schmidt-Supprian, M. Pasparakis, R. Beyaert, and G. van Loo. 2010. Enterocyte-specific A20 deficiency sensitizes to tumor necrosis factor-induced toxicity and experimental colitis. *J. Exp. Med.* 207:1513–1523. https://doi.org/10.1084/jem.20092474

Vereecke, L., S. Vieira-Silva, T. Billiet, J.H. van Es, C. Mc Guire, K. Slowicka, M. Sze, M. van den Born, G. De Hertogh, H. Clevers, et al. 2014. A20 controls intestinal homeostasis through cell-specific activities. *Nat. Commun.* 5:5103. https://doi.org/10.1038/ncomms6103

Vivier, E., E. Tomasello, M. Baratin, T. Walzer, and S. Ugolini. 2008. Functions of natural killer cells. *Nat. Immunol.* 9:503–510. https://doi.org/10.1038/ni1582

Vivier, E., S. Ugolini, D. Blaise, C. Chabannon, and L. Brossay. 2012. Targeting natural killer cells and natural killer T cells in cancer. *Nat. Rev. Immunol.* 12:239–252. https://doi.org/10.1038/nri3174

Vivier, E., D. Artis, M. Colonna, A. Diefenbach, J.P. Di Santo, G. Eberl, S. Koyasu, R.M. Locksley, A.N.J. McKenzie, R.E. Mebius, et al. 2018. Innate Lymphoid Cells: 10 Years On. *Cell.* 174:1054–1066. https://doi.org/10.1016/j.cell.2018.07.017

Vosshenrich, C.A.J., T. Ranson, S.I. Samson, E. Corcuff, F. Colucci, E.E. Rosmaraki, and J.P. Di Santo. 2005. Roles for common cytokine receptor gamma-chain-dependent cytokines in the generation, differentiation, and maturation of NK cell precursors and peripheral NK cells in vivo. *J. Immunol.* 174:1213–1221. https://doi.org/10.4049/jimmunol.174.3.1213

Waggoner, S.N., S.D. Reighard, I.E. Gyurova, S.A. Cranert, S.E. Mahl, E.P. Karmele, J.P. McNally, M.T. Moran, T.R. Brooks, F. Yaqoob, and C.E. Rydyznski. 2016. Roles of natural killer cells in antiviral immunity. *Curr. Opin. Virol.* 16:15–23. https://doi.org/10.1016/j.coviro.2015.10.008